

Strong nonlocal tuning of the current-phase relation of a quantum dot based Andreev moleculeMátyás Kocsis^{1,2,*}, Zoltán Scherübl^{1,2}, Gergő Fülöp^{1,2}, Péter Makk^{1,3} and Szabolcs Csonka^{1,2,4}¹*Department of Physics, Institute of Physics, Budapest University of Technology and Economics, Műegyetem rkp. 3., H-1111 Budapest, Hungary*²*MTA-BME Superconducting Nanoelectronics Momentum Research Group, Műegyetem rkp. 3., H-1111 Budapest, Hungary*³*MTA-BME Correlated van der Waals Structures Momentum Research Group, Műegyetem rkp. 3., H-1111 Budapest, Hungary*⁴*Institute of Technical Physics and Materials Science, HUN-REN Centre for Energy Research, Konkoly-Thege Miklos út 29-33., H-1121 Budapest, Hungary*

(Received 17 January 2024; revised 21 May 2024; accepted 22 May 2024; published 25 June 2024)

Recent realization of minimal Kitaev chains brought a breakthrough in Majorana research, which made arrays of quantum dots coupled by superconductor spacers the most promising synthetic quantum material for topological quantum architectures. In this paper, we investigate the basic building block of this platform—two dots coupled via a superconductor (referred to as an Andreev molecule)—in a configuration where two superconducting (SC) loops are created to tune the SC phase difference across the dots. This enables us to consider Coulomb interactions which was not possible in previously studied systems. We demonstrate that the Andreev molecule shows a strong nonlocal Josephson effect: As the dot in one junction is tuned, the current-phase relation (CPR) of the other dot is modified. This architecture hosts $0-\pi$ transitions and shows a tunable anomalous φ_0 phase shift, nonlocally controlled in both cases, without relying on spin-orbit interaction or Zeeman fields used in previous studies. In addition, a significant SC diode effect and π -periodic CPRs can be observed. The presented nonlocal CPR can be used as a signature of the formation of an Andreev molecular state and in general to introduce ways to tune quantum architectures.

DOI: [10.1103/PhysRevB.109.245133](https://doi.org/10.1103/PhysRevB.109.245133)**I. INTRODUCTION**

Hybrid superconductor-semiconductor structures are the subject of surging fascination since they can serve as synthetic quantum materials hosting non-Abelian excitations [1–5] and provide topological protection in quantum computational applications [6,7]. One of the most promising synthetic quantum materials is the Kitaev chain [8], shown in Fig. 1(a), consisting of a chain of quantum dots (QDs) coupled by superconducting (SC) spacers. The smallest version of such a chain is two QDs connected to an SC link, a minimal Kitaev chain hosting states referred to as *poor man's Majorana* states [9–11]. A similar minimal setup is also used for splitting Cooper pairs (CPs) [12–18], where the SC-QD coupling is usually weak. However, when a QD is coupled to an SC, so-called *Andreev bound states* (ABSs) form, which have been widely studied [19–35]. When two sites hosting such ABSs are closely spaced, the ABSs hybridize and form an Andreev molecular state, as described in weak links [36,37], coupled QDs [38], and even in multiterminal SC devices [39–41]. Recent advancements of nanofabrication allowed the demonstration of signatures of such Andreev molecules [41–43], and very recently, the observation of poor man's Majorana modes has also been shown [11].

In this paper, we study the minimal Kitaev chain coupled to two outer SC leads, as shown by the red dashed rectangle in

Fig. 1(a). This configuration allows the application of phase biases (φ_L, φ_R) on the two QDs as well as modifying the level position ($\varepsilon_L, \varepsilon_R$) of the dots [see Fig. 1(b)], enabling us to examine the role of Coulomb interactions in an Andreev molecule. We will show that the presence of the Andreev molecular state induces a strong nonlocal current-phase relationship (CPR) on the dots.

Specifically, we study a device shown in Fig. 1(b), two QDs (black) embedded in one SC loop (blue) each, where the two loops share a side. Two flux lines (green) can be used to apply arbitrary magnetic flux into the SC loops to control the SC phase differences across the QDs (φ_L, φ_R). Adding two side gates (orange) allows us to electrostatically control the on-site energy of the two QDs separately ($\varepsilon_L, \varepsilon_R$). This control is not possible if the Josephson junctions (JJs) behave as noninteracting transport channels [36,37]. As we will show, this distinction leads to interesting behavior in our system.

In the following sections, we show how this device behaves in different parameter regimes and what robust signatures of the Andreev molecular states can be observed. The Andreev molecular states are observed through the presence of the nonlocal Josephson effect, where the supercurrent flowing through one dot is influenced by tuning the parameters of the other QD. We demonstrate $0-\pi$ and large φ_0 phase shifts even in the absence of ground-state (GS) change. Here, π -periodic CPRs are also demonstrated for certain parameter configurations. Unlike previous systems [44–53], ours does not rely on spin-orbit interaction (SOI) or a Zeeman field. This makes such devices especially suited for applications where φ_0

*Corresponding author: matyaskocsis@edu.bme.hu

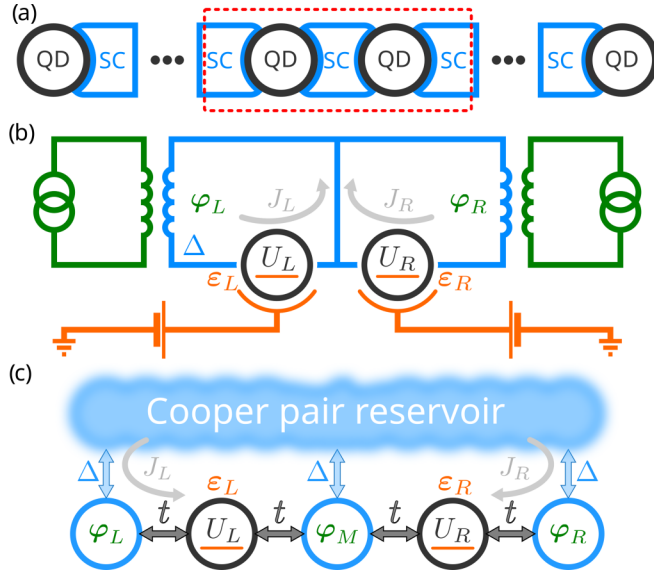


FIG. 1. (a) A chain of quantum dots (QDs) connected by superconductors can host Majorana fermions. Three superconducting (SC) sites connected by QDs (dashed red line) can be thought of as a basic building block of such a system. (b) The proposed circuit for studying Andreev molecules, two SC quantum interference devices (SQUIDs) with a QD in each Josephson junction, which allow phase biasing (φ_L, φ_R) across either dot. By gating the QDs, and phase-biasing the loops separately, we have four individually tunable variables. The gray arrows show the currents flowing in the SC loops. (c) Five-site model used in our calculations. We set the SC phase of the middle site to $\varphi_M = 0$ in all cases. For simplicity, we keep all t hopping terms equal, and set $U_L = U_R = U = 1$ as our energy scale, with $\Delta = 0.4U$ in all calculations.

junctions have been considered, such as phase batteries [54,55]. We also demonstrate a considerable nonlocally tunable SC diode effect.

II. METHODS

The phase-biased Andreev molecule system was modeled with a chain of five sites, as shown in Fig. 1(c), denoted as SC_L - QD_L - SC_M - QD_R - SC_R , with all sites coupled to their nearest neighbors. The left and right QDs are labeled with L and R, while the SC sites are labeled L, M, and R for the left, middle, and right site respectively. The coupling strength between nearest neighbors (t) is kept the same across the system, it is scaled with the Coulomb energy of the dots ($U = U_L = U_R = 1$), and so are the on-site energies of the dots ($\varepsilon_R, \varepsilon_L$).

The Hamiltonian describing the system can be written as

$$H = H_{\text{QD}} + H_{\text{SC}} + H_{\text{NN}}, \quad (1)$$

where H_{QD} contains the terms related to the QDs, H_{SC} the terms related to the SC sites, and H_{NN} describes the nearest-neighbor tunnel couplings.

We assume that the level spacing of the QDs are large, so each QD can be modeled with a single spinful orbital. The

QDs are treated according to the Anderson model:

$$H_{\text{QD}} = \sum_{\alpha=\text{QD}_L, \text{QD}_R} \varepsilon_{\alpha} \hat{n}_{\alpha} + U_{\alpha} \hat{n}_{\alpha, \uparrow} \hat{n}_{\alpha, \downarrow}, \quad (2)$$

where ε_{α} is the on-site energy, and U_{α} is the on-site Coulomb repulsion energy. For the number operator of the QDs, $\hat{n}_{\alpha} = \sum_{\sigma=\uparrow, \downarrow} \hat{n}_{\alpha, \sigma}$, where $\hat{n}_{\alpha, \sigma} = \hat{c}_{\alpha, \sigma}^{\dagger} \hat{c}_{\alpha, \sigma}$, the operators $\hat{c}_{\alpha, \sigma}$ and $\hat{c}_{\alpha, \sigma}^{\dagger}$ are the annihilation and creation operators on site α .

When describing the SC leads, we approximate the full BCS Hamiltonian using the zero-bandwidth (ZBW) approximation [56,57], where an SC site can only host a single quasiparticle (QP) at energy $\pm \Delta$. We use the ZBW approximation, as it has been shown to yield results that compare quantitatively with the outcome of numerical renormalization group (NRG) calculations, when care is taken in choosing the scale of the SC gap and the couplings, describing QDs attached to SCs [56–58]. The ZBW Hamiltonian of the SC sites takes the form:

$$H_{\text{SC}} \approx H_{\text{ZBW}} = \sum_{\alpha=\text{SC}_L, \text{SC}_M, \text{SC}_R} \Delta (\exp(i\varphi_{\alpha}) \hat{c}_{\alpha, \uparrow}^{\dagger} \hat{c}_{\alpha, \downarrow}^{\dagger} + \text{H.c.}), \quad (3)$$

where Δ is the SC gap, and φ_{α} is the SC phase of the site. Since the SC phase is transferable from one SC site to another via simple gauge transformations, we set the SC phase on the middle SC site to zero, $\varphi_M = 0$.

The nearest-neighbor coupling is expressed as

$$H_{\text{NN}} = \sum_{(\alpha, \beta)} t_{\alpha, \beta} (\hat{c}_{\alpha, \uparrow}^{\dagger} \hat{c}_{\beta, \uparrow} + \hat{c}_{\alpha, \downarrow}^{\dagger} \hat{c}_{\beta, \downarrow} + \text{H.c.}), \quad (4)$$

where $t_{\alpha, \beta}$ describes the strength of the coupling between neighboring sites.

We only consider terms diagonal in spin, representing spin-conserving tunneling, as the system we consider lacks SOI. How SOI could be incorporated into the model is discussed in Ref. [38]. For simplicity, we use $t_{\alpha, \beta} = t$ for all α and β . In general, our findings are applicable even if the values of $t_{\alpha, \beta}$ are not precisely matched; asymmetries in the coupling are discussed in Appendix A.

To make sure that the use of the ZBW approximation is valid, we always set $t < \Delta < U$. Unless indicated otherwise, in all calculations, $t = 0.2U$ and $\Delta = 0.4U$. By using Eq. (3) instead of a full BCS Hamiltonian to describe the SC sites, Eq. (1) becomes finite dimensional, so it can be diagonalized numerically.

In similar systems with only one QD, the current is calculated using the derivatives of the free energy [57]. In our case, however, there are two different supercurrents of interest, shown by the light gray arrows in Figs. 1(c) and 1(b). Here, J_R flows in the right loop through the right SC site, and J_L flows in the left loop through the left SC site. Once the energy spectrum and the eigenstates of the full Hamiltonian are calculated, we consider a stationary solution, where the incoming and outgoing flows of particles add up to zero on every site, so

$$i\hbar \partial_t \hat{n}_{\alpha} = [\hat{n}_{\alpha}, H] = 0. \quad (5)$$

Applying these formulas to the SC site on the right, we get

$$i\hbar \partial_t \hat{n}_{\text{SC}_R} = [\hat{n}_{\text{SC}_R}, H] = [\hat{n}_{\text{SC}_R}, H_{\text{ZBW}}] + [\hat{n}_{\text{SC}_R}, H_{\text{NN}}]. \quad (6)$$

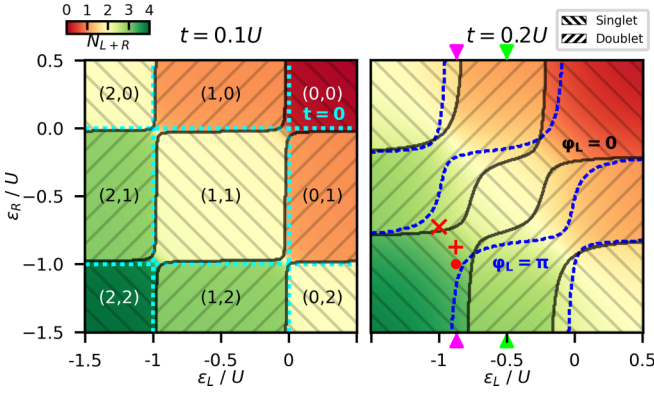


FIG. 2. Stability diagrams at different coupling strengths. The colors show the overall particle number as a function of the on-site energy of the two quantum dots (QDs), ε_L , ε_R . The parity of the ground state is indicated by hatching; the solid black line denotes the singlet-doublet boundary. (a) Weaker coupling, $t = 0.1U$. The cyan dotted line shows the singlet-doublet boundary without any coupling; labels show the occupation numbers of left and right QDs. With nonzero coupling, the regions with the same parity hybridize. The former (1,1) region shrinks due to the coupling. (b) Stronger coupling, $t = 0.2U$. The hybridized regions expand; the region where (1,1) is the dominant particle number configuration shrinks further. The blue dotted line shows the singlet-doublet boundary when a magnetic flux is inserted into the left loop, $\varphi_L = \pi$. In all other cases, no magnetic flux is present, $\varphi_L = \varphi_R = 0$.

The terms in Eq. (6) are also shown in Fig. 1(c) and can be thought of as the particle current flowing into the SC site from the CP reservoir [right blue vertical arrow in Fig. 1(c)] described by the term containing H_{ZBW} and the particle current flowing into the site through the coupling to the neighboring QD [right dark gray horizontal arrow in Fig. 1(c)] described by the term containing H_{NN} . According to Eq. (5), these currents should be equal with opposing signs:

$$[\hat{n}_{SC_R}, H_{ZBW}] = -[\hat{n}_{SC_R}, H_{NN}] = i\hbar\hat{J}_R, \quad (7)$$

where \hat{J}_R is the operator of the current flowing through the right SC site. This enables us to study J_R and J_L separately as well as the CPRs of our system and show signatures of the Andreev molecular state. We neglect H_{QD} in these equations, as it does not influence the SC sites.

In this paper, we consider the GS of the system, which can be divided into even and odd phases, depending on the total number of electrons on the QDs. This particle parity gives a useful tool to explore how the stability diagram of our system is influenced by the strength of the coupling between sites. It is important to note that we always consider the whole system; thus, if both QDs have odd occupancy, the system as a whole is still considered to be in an even state.

III. RESULTS

A. Phase diagram

First, let us illustrate [see Fig. 2(a)] how the localized ABSs residing on separate dots hybridize into a molecular one by studying the charge stability diagram of the system with relatively weak $t = 0.1U$ coupling. The two axes correspond

to the on-site energy of the left and right QDs, the colors show the number of particles in the whole system consisting of two QDs, which can range from 0 to 4. We label the different regions with particle numbers of the left and right QD (n_L, n_R) which, in the absence of couplings (i.e., $t = 0$), would be exact. Region boundaries of the noninteracting case are marked by the dotted cyan lines in Fig. 2(a). With nonzero coupling strength, we still have regions where the labeled states are good approximations of the GS; however, the boundaries are shifted as marked by the solid lines. The hatching denotes the odd and even parity regions, as discussed in Sec. II. For example, the top right region corresponds to both dots being empty, hence the (0,0) label, and the hatching denotes the even states. Since we do not apply any Zeeman field and the system has no SOI, the energy levels of the QDs are spin degenerate. For example, the state (0,↑) has the same energy as (0,↓). The even-parity GS is always a singlet, while the odd-parity GS is a spin-degenerate doublet, so we use the words singlet (doublet) and even (odd) interchangeably to describe the different regions.

In Fig. 2(a), there are small regions around the corners of the (1,1) charge region where we can see the effects of coupling the QDs to the SC sites as avoided crossings. This coupling shrinks the doublet regions, e.g., the solid borders of the (1,0), (0,1) regions are shifted inward from the dotted lines, where they meet. This is also true for the (2,1) and (1,2) regions since single occupancy of the QDs becomes less favored due to the presence of SC correlations on the QDs [59,60]. Regions with the same parity start hybridizing, e.g., the (0,0), (1,1), and (2,2) regions of even parity are connected, while the odd (1,0) state connects with the (2,1) state. This is the consequence of crossed Andreev reflection (CAR), where a CP from the middle SC site is split up, and one electron enters the left and right QDs each. This process couples the localized ABSs residing on the separate dots to form the molecular Andreev states.

As the strength of the coupling increases, the doublet regions shrink further, while the hybridized regions expand, as shown in Fig. 2(b) for $t = 0.2U$. Comparing the solid lines on the lower part ($\varepsilon_R < U$) of the two panels of Fig. 2, we see that the doublet region contracted from spanning the middle half of the axis ($\varepsilon_L \approx -1U$ to $\varepsilon \approx 0$) to less than a third, while the hybridized region of the former (1,2) and (0,1) states expanded significantly.

So far, no SC phase difference was present across the junctions ($\varphi_L = \varphi_R = 0$); however, our systems allow for individually phase-biasing each junction. To demonstrate the effect of flux-biasing one of the JJs, we show the singlet-doublet boundary for the $\varphi_L = \pi$, $\varphi_R = 0$ case with a dashed blue line in Fig. 2(b), where the changes are the most pronounced. Examining the lower part of Fig. 2(b) again, we see that the doublet region has expanded along ε_L , as $\varphi_L = 0 \rightarrow \pi$. In contrast, the vertical extension of the (0,1) doublet region at $\varepsilon_L = 0.5U$ (right side of the panel) is not affected. Thus, remarkably, in some regions (e.g., at the point marked with a red \times), a quantum phase transition can be induced, i.e., a GS parity change can be induced by tuning the SC phase. Similar quantum phase transitions, tuned by the SC phase, have been recently observed in simpler SC-QD-SC systems [60]. In addition to investigating the GS properties of the

Andreev molecular states, we also evaluated its excited state spectra, which is described in Appendix D.

While the charge stability diagrams are useful for understanding the behavior of the system, experimentally detecting nonlocal effects is most straightforward by measuring the supercurrent flowing through one of the QDs. In the following, we will focus on the CPR of the right QD and show experimental signatures of the molecular state. We will refer to φ_R and ε_R parameters as local, while referring to φ_L and ε_L as nonlocal. The same effects could also be observed with the roles reversed. For detailed comparisons of J_L and J_R , see Appendix B.

First, we will discuss the case when the nonlocal QD is off-resonant and our device resembles the simpler SC-QD-SC devices [60]. This yields a $0-\pi$ transition when the GS changes parity, very similar to the one in the SC-QD-SC setup. We then move on by tuning the nonlocal QD to resonance and showing a $0-\pi$ phase shift of the CPR, in the absence of GS parity change. Then we present how this $0-\pi$ phase shift appears whenever the SC phase across the nonlocal junction is an integer multiple of π ($\varphi_L = k\pi$). Along the way, we will find that the system can be tuned such that π -periodic CPRs can be observed. Finally, the case of arbitrary φ_L is also considered, where we find a tunable φ_0 phase shift.

B. CPRs

1. Off-resonance case

The left QD is tuned far from hybridization between the QDs by tuning ε_L so that the left QD is deep in blockade. The green arrows in Fig. 2(b) show one such value for ε_L , equidistant from both resonances at $\varepsilon_L = -0.5U$. The CPR for some values of ε_R is shown in Fig. 3(a), while Fig. 3(b) shows the same for a wide region of ε_R . The particular values of ε_R , where the line cuts of Fig. 3(a) are taken, are indicated by arrows.

The orange and blue curves of Fig. 3(a) show a near sinusoidal CPR corresponding to a conventional 0 junction (skewness and higher harmonic components of the CPRs are addressed in Appendix C), taken at $\varepsilon_R = -1.396U$ and $\varepsilon_R = -1.018U$, respectively. In this region, the GS is a doublet state, as opposed to SC-QD-SC systems where the 0 junction is in the singlet region [60]. This is due to the single electron occupying the off-resonance nonlocal QD, which does not influence the local current but is counted when determining the particle parity of the whole system, as discussed in Sec. II.

The green ($\varepsilon_R = -0.737$) and red ($\varepsilon_R = -0.496$) curves show CPRs which are shifted by π in φ_R corresponding to a π junction. The $0-\pi$ transition is driven by the GS transition, yielding a parity change [as demonstrated by the coincidence of the blue-red color transition and the solid black phase boundary in Fig. 3(b)]. This means that we need to add or remove a QP to/from the system to observe the $0-\pi$ transition. As expected, these results show the same qualitative behavior as a single SC-QD-SC system [60] since the left QD is in blockade.

2. Hybridization, $\varphi_L = 0$

Tuning the nonlocal QD toward the hybridization region has very striking effects on the CPRs, for example, by setting

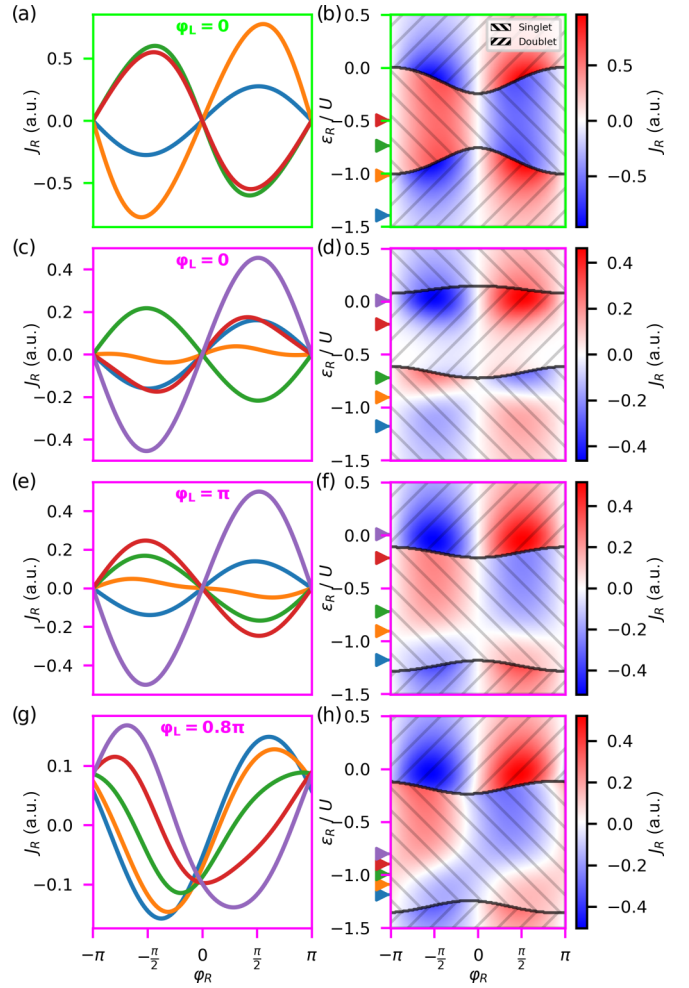


FIG. 3. Current-phase relation (CPR) of the local quantum dot (QD). The left column shows curves at some given local on-site energy ε_R ; the right shows CPR dependence on the on-site energy. Colors represent the local supercurrent J_R ; hatching indicates the singlet and doublet regions; and solid lines indicate the phase boundary. Arrows indicate the values of ε_R where the curves on the left were taken. (a) and (b) Nonlocal QD is deep in blockade. Blue and green curves show a $0-\pi$ transition, the parity of the ground state (GS) changes. (c) and (d) Nonlocal QD is on resonance and $\varphi_L = 0$. Blue and green curves show a $0-\pi$ transition, surprisingly without the need for parity change in the GS. (e) and (f) Nonlocal QD is on resonance, with $\varphi_L = \pi$. The blue and green curves show a $0-\pi$ transition, without GS parity change like the case above. Singlet and doublet phases are inverted; the transition still takes place in the singlet region. (g) and (h) Nonlocal QD is on resonance, its superconducting (SC) phase is a noninteger multiple of π ($\varphi_L = 0.8\pi$). Curves show a φ_0 phase shift; the maximum is continuously shifted with local on-site energy ε_R . This φ_0 transition relies only on the nonlocal phase tuning and does not require spin-orbit interaction.

$\varepsilon_L = -0.87U$, as shown by the magenta arrow in Fig. 2(b). Figure 3(c) shows some CPR curves taken at this position. Comparing the red and green curves, we see a $0-\pi$ transition which is accompanied with a GS parity change, as before. Comparing the blue and green curves, we see that a $0-\pi$ phase shift takes place. However, in strong contrast to the previous example, it is not accompanied by a GS parity change.

Figure 3(d) shows the phase shift between the blue and green arrows taking place entirely in the singlet sector, which is a direct consequence of the Andreev molecular state spanning the two QDs. Whenever $0-\pi$ phase shifts take place without a change in GS parity, CPR curves with dominant higher harmonic elements can be observed, as shown by the orange curve of Fig. 3(c). Similar behavior has been predicted and measured in asymmetric $0-\pi$ Josephson junctions consisting of two parallel junctions [47,48] or in balanced SC quantum interference devices (SQUIDS) [61–63]. In contrast to these devices, which were only tunable by changing the device geometry or by a Zeeman field, in our case, the phase shift is tuned by local gating.

By choosing all parameters carefully, the CPR can take a close-to- π -periodic form in φ_R , as shown by the orange curve of Fig. 3(d), and can serve as a unique signature of Andreev molecular states. Recently proposed protected qubits are based on systems with $\cos 2\varphi$ CPRs [64]. Tuning our system such that the first harmonic part of the CPR is totally suppressed, thus leading to an ideal π -periodic junction, is also possible. The details of such π -periodic CPRs and protected qubits are discussed in Appendix C.

Interestingly, the other GS parity change around $\varepsilon_R \simeq 0$ is not accompanied by a $0-\pi$ transition; rather, a $0-0'$ transition is taking place, with a significant drop in the amplitude of J_R entering the singlet sector.

3. Hybridization, $\varphi_L = \pi$

By tuning the nonlocal flux to $\varphi_L = \pi$, we see a dramatic shift of the CPRs from that of Figs. 3(d)–3(f). Such dramatic dependence of the local CPR on the nonlocal flux is also a characteristic signature of the Andreev molecular state. To understand how this change manifests, we come back to the stability diagram.

When comparing the blue dashed line of Fig. 2 corresponding to $\varphi_L = \pi$, with the solid lines corresponding to $\varphi_L = 0$, we see that the singlet and doublet regions have flipped. Now the central region is a singlet hybrid of the (2,2) and (1,1) states, and the outer regions are in doublet GSs. This inversion of the parity regions is most notable when comparing the hatching of Figs. 3(d) and 3(f). The CPR curves in Fig. 3(e) show the same $0-\pi$ phase shift without a GS transition as discussed earlier (see blue and green curves). The orange curves of Figs. 3(c) and 3(e) show similar close-to- π -periodic CPRs in the singlet sector.

4. φ_0 phase-shift

In all cases discussed so far, the nonlocal phase was either 0 or π ; however, tuning φ_L to noninteger multiples of π can yield exciting features. This is demonstrated in Figs. 3(g) and 3(h) for $\varphi_L = 0.8\pi$, where instead of a $0-\pi$ phase shift, the phase of the CPRs in the singlet region is shifted by an arbitrary phase φ_0 .

Josephson junctions in which the critical current takes on an anomalous phase, such that $J_c = J_0 \sin(\varphi + \varphi_0)$, have been studied both theoretically and experimentally [44–51] and are great candidates for the creation of phase batteries [54,55]. In some cases, the value of φ_0 is even tunable [52,53,55]. However, in all cases, SOI or a Zeeman field is required. In our

case, neither SOI nor external fields are required to produce this anomalous phase shift and tune the value of φ_0 . This tunable phase shift in the absence of SOI or external fields is a strong indicator of the presence of Andreev molecular states.

In systems with a single junction, time-reversal symmetry (TRS) dictates that $J(\varphi) = -J(-\varphi)$, which implies that $J(\varphi = 0) = 0$. The presence of an anomalous Josephson current $J(\varphi = 0) \neq 0$ can only occur if SOI is present and TRS is broken, for example, by a Zeeman field [51].

For our double-junction system, TRS dictates that $J(\varphi_L, \varphi_R) = -J(-\varphi_L, -\varphi_R)$ [36], which in the case of $\varphi_L = k\pi$ simplifies to $J(\varphi_R) = -J(-\varphi_R)$. The vertical white bands in the middle of Figs. 3(b), 3(d) and 3(f) at $\varphi_R = 0$ show this symmetry. If φ_L is set to an arbitrary value, $J(\varphi_R = 0) = 0$ no longer holds true. This effect is demonstrated in Figs. 3(g) and 3(h) for $\varphi_L = 0.8\pi$, where a φ_0 phase shift is observed in the singlet region. The anomalous phase φ_0 is also strongly tunable by local gating.

Having a noninteger multiple of π as the nonlocal phase also introduces significant changes in the shape of the CPR curves. The CPR curves shown up to now all had symmetry where the absolute value of the minimal and maximal supercurrent was equal $|\max[J_R(\varphi_R)]| = |\min[J_R(\varphi_R)]|$ [see Figs. 3(a), 3(c) and 3(e)]. For the curves of Fig. 3(g), however, $|\max[J_R(\varphi_R)]| \neq |\min[J_R(\varphi_R)]|$, with the green curve showing the strongest effect (with the absolute value of the minimum and maximum showing a 28% difference). This effect is referred to as the SC diode effect [44,65–73], which is observed in systems where both inversion symmetry and TRS are broken. In our system, the TRS is broken by phase biasing, and the spatial symmetry is broken from the perspective of QD_R . These symmetry breaks are nonlocal due to the spatial extension of the GS wave function over the two dots [72].

5. Nonlocal phase tuning

All three effects discussed so far are signatures of the Andreev molecular states formed in the QDs. Since tuning the nonlocal phase has such a fundamental effect on the system, we will study the φ_0 and $0-\pi$ phase shifts in more detail as a function of the nonlocal phase. We then show a third scenario where the nonlocal phase drives a singlet-doublet transition.

By fixing the on-site energies to the values indicated in Fig. 2 by a red dot, we can study how the nonlocal phase φ_L tunes the φ_0 shift of the local CPR. Figure 4(a) shows a few selected CPR curves at different values of φ_L , demonstrating the φ_0 junctionlike behavior. The exact phase shift can be tuned in a wide range by the nonlocal phase. When both local and nonlocal phases are zero, the current is completely suppressed.

Mirroring Fig. 4(b) around the $\varphi_L = 0, \varphi_R = 0$ point and inverting the colors yields the original figure. This is a consequence of TRS mentioned earlier, which implies that $J(\varphi_L, \varphi_R) = -J(-\varphi_L, -\varphi_R)$ [36].

A π phase shift controlled by the nonlocal phase is also achievable by tuning the dots such that $\varepsilon_L = \varepsilon_R$, as shown by the red + in Fig. 2. Figures 4(c) and 4(d) show the local current reversal by nonlocal phase. The nonlocal phase switches the junction from a 0 to a π phase shift, as the blue

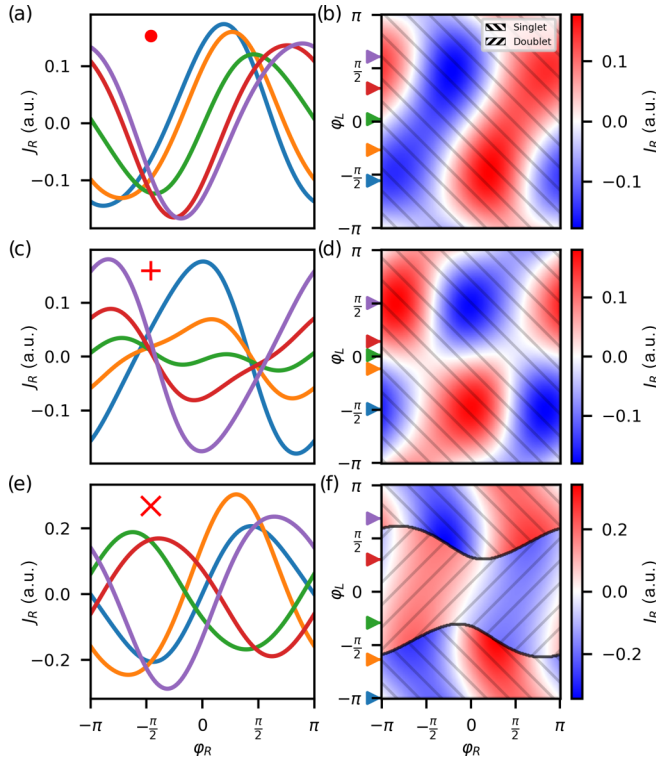


FIG. 4. Current-phase relation (CPR) of the local quantum dot (QD), as a function of the nonlocal superconducting (SC) phase φ_L . The nonlocal phase tuning of the local supercurrent is the nonlocal Josephson effect. The on-site energies where the CPRs are taken are marked with corresponding red marks in Fig. 2. The left column shows curves at some given nonlocal SC phase values φ_L , while the right column shows how CPR depends on the nonlocal SC phase in a continuous window. (a) and (b) φ_0 phase shift, tuned by nonlocal phase. The curves are continuously shifted by the nonlocal phase. The absolute value of the minimum and maximum current differs for each curve, showing the SC diode effect. This is true for all on-site energy configurations shown here. (c) and (d) $0-\pi$ phase shift, tuned by nonlocal phase, without requiring the change of ground state (GS) parity. Close to the transition, the CPR is strongly nonsinusoidal. (e) and (f) The quantum phase transition of the GS from the singlet to the doublet state is driven by the nonlocal phase. Within the same parity regions, φ_0 phase shift is observable, while $0-\pi$ transitions take place along the singlet-doublet boundary.

and purple curves show, without changing the parity of the GS. The change from the φ_0 to the $0-\pi$ regime is detailed in Sec. IV.

It is also possible to drive GS transition between the singlet and doublet GSs by nonlocal flux tuning, as shown in Figs. 4(e) and 4(f). To achieve this, we set the on-site energies of the QDs close to the boundary, as shown in Fig. 2 by a red \times . The GS switch also means a $0-\pi$ transition, while within a given GS, the nonlocal phase has a φ_0 -like behavior. Comparing the red and green curves of Fig. 4(e), we see that the SC diode effect has the same strength, but the polarity is flipped. This means that, in this regime, the system can be used as an SC diode in which the strength and the polarity of the effect is easily tunable.

IV. DISCUSSION

Let us now compare our QD-based Andreev molecule with a system with the same geometry but where the JJs are modeled as noninteracting channels [36,37]. There are three phenomena discussed in this paper that are also present in the noninteracting-channel-based model. These are the breaking of the $J_R(\varphi_R = 0) \neq 0$ symmetry, the SC diode effect, and the tunable φ_0 phase shift. In addition to being able to control the φ_0 shift of the transition via the nonlocal phase φ_L [Figs. 4(b) and 4(f)], our system allows it to be controlled via the local gate voltage (on-site energy) ε_R [Fig. 3(h)] as well, in stark contrast with the noninteracting case. It is important to note that our model does not consider the distance between the two junctions, which is an important parameter of the experimental realization.

The $0-\pi$ phase shift without changing GS parity is absent in the noninteracting model; it is unique to our QD-based one. These are markedly different from $0-\pi$ transitions where the GS parity changes: There exists a central region between the 0 and π phases where the CPR is nonsinusoidal and the amplitude of the supercurrent is low, as opposed to the sharp changes characteristic of GS-changing transitions. This holds true whether the transition is tuned by the local on-site energy ε_R [Figs. 3(d) and 3(f)] or the nonlocal phase φ_L [Fig. 4(d)].

In this paper, we have studied a QD-based Andreev molecule between SC leads. We explored its characteristics for different level positions of the dots and different phase biasing of the JJs, which led to unusual and strongly varying CPRs due to the molecular hybridization.

Our proposed circuit can be fabricated from state-of-the-art semiconductor-superconductor nanostructures, like nanowires with an epitaxial Al shell that is etched away to form the QDs or 2DEG systems proximitized with an epitaxial Al layer. Both platforms have been used experimentally to create similar devices [42,74–77], showing the feasibility of the realization of the device concept under investigation. The semiconductor can be depleted by local gating, which allows the characterization of a single JJ at a time. Local gating can tune the energy level of the QD in the presence of Coulomb interactions, which has been crucial in many recent experiments as well [42,74,75]. The supercurrents can be measured using high-frequency techniques, commonly used in measuring similar devices [60,74,76,78]

We demonstrated how tuning the nonlocal QD away from Coulomb blockade results in $0-\pi$ or φ_0 phase shift of the CPR of the local JJ. The nonlocal Josephson effect is demonstrated by showing how the nonlocal flux can influence the behavior of the local current. This yields $0-\pi$ and φ_0 phase shifts as well. Contrary to the single-dot case, the nonlocally controlled $0-\pi$ and φ_0 phase shifts can occur without QP parity changes, and a significant and highly tunable SC diode effect is also demonstrated.

Unlike devices that show similar behavior, our system does not rely on Zeeman fields or SOI. Our results show that these effects can be observed in a wide parameter range. This makes the system valuable for studying both the SC diode effect and the applications of a programmable φ_0 junction. The strong nonlocal tuning of the CPR is a hallmark of the Andreev

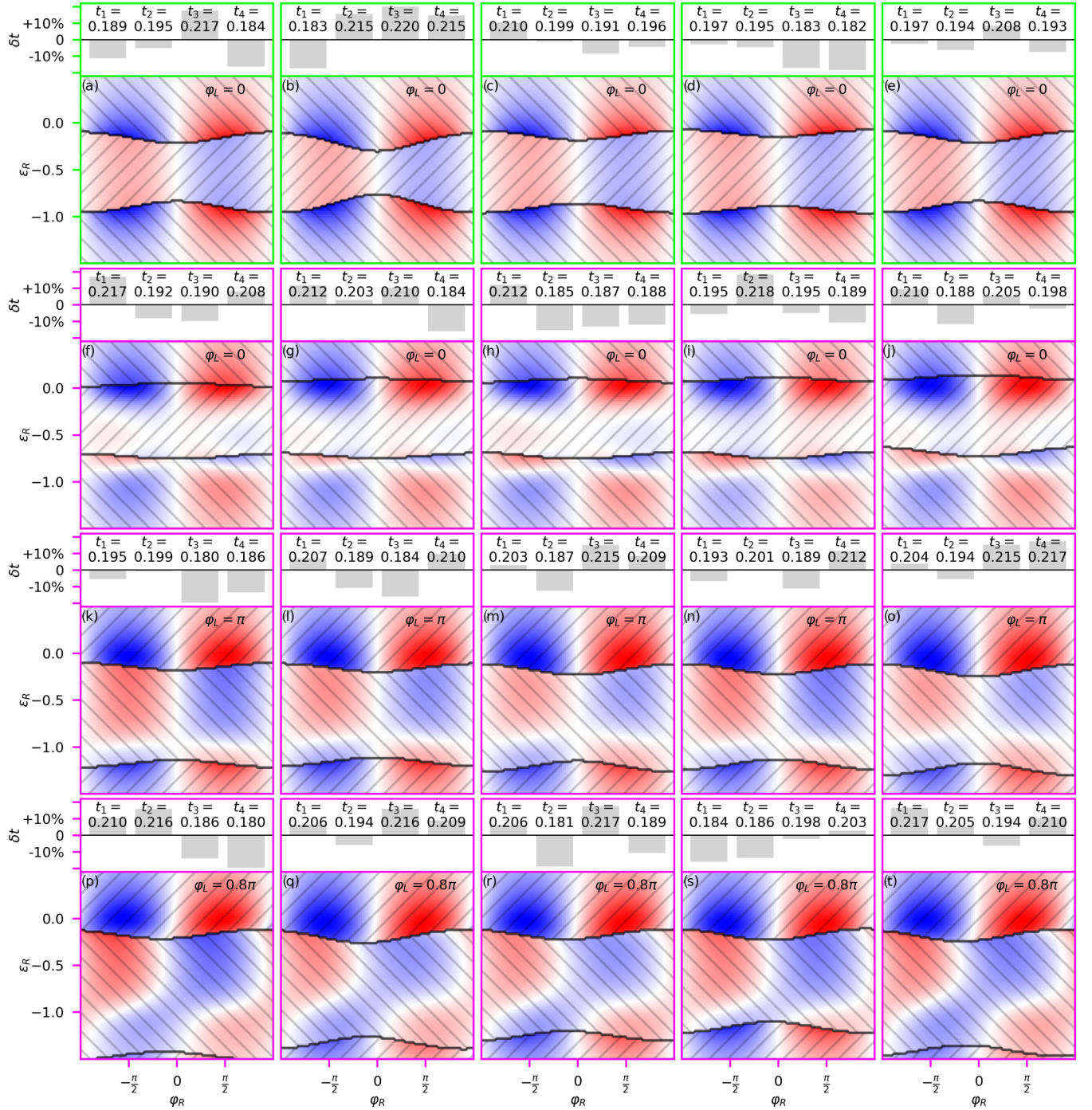


FIG. 5. Local current J_R as a function of the local phase φ_R and the local on-site energy ε_R , at the same nonlocal phase φ_L and nonlocal on-site energy ε_L values as Fig. 3. Each row represents a parameter setting, with the couplings $t_{\alpha,\beta}$ randomized within a $\pm 20\%$ range five times. The main features discussed in the main text are conserved even for randomized couplings; they are not a consequence of symmetric values of $t_{\alpha,\beta}$. The color scales of each panel are normalized individually; the colors of different panels are not comparable.

molecular state, which is promising for future quantum architectures, like protected qubits.

In this paper, we studied the GS properties of the system. Studying the excitation spectrum may reveal further experimentally observable features of the Andreev molecular state.

Note added. It has come to our attention that, due to high interest in the field, during the preparation of this manuscript, multiple studies have been carried out [72,79–82].

All data are available upon request from the author.

ACKNOWLEDGMENTS

The authors declare no competing financial or nonfinancial interests. This paper has received funding from SuperGate Fet Open, the FET Open AndQC, Twistrain ERC, and from the OTKA Grants No. FK-132146, No. K-138433, and No. K-134437. This paper was supported by the Ministry of Culture

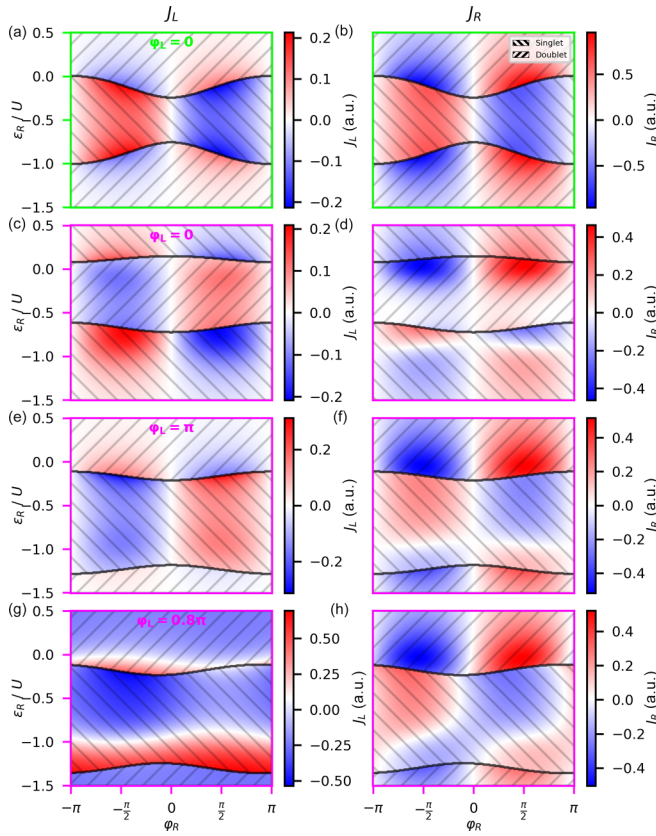


FIG. 6. The current of the nonlocal junction J_L and the local junction J_R , as a function of the local phase φ_R and the local on-site energy ε_R . For each row, the nonlocal parameters φ_L and ε_L are the same as for the same row of Fig. 3.

and Innovation and the National Research, Development and Innovation Office within the Quantum Information National Laboratory of Hungary (Grant No. 2022-2.1.1-NL-2022-00004), Grant No. TKP2021-NVA-02, by the ÚNKP-22-5, and the ÚNKP-23-5-BME-413 New National Excellence Program of the Ministry for Culture and Innovation from the source of the National Research, Development and Innovation Fund, the János Bolyai Research Scholarship of the Hungarian Academy of Sciences, and the EIC Pathfinder Challenge grant QuKiT (Grant No. 101115315).

M.K. developed the simulations with the help of G.F. and Z.S. M.K. ran the simulations and visualizations. P.M. and Sz. Cs. supervised the work. All authors analyzed and discussed the results and contributed to the manuscript.

APPENDIX A: ASYMMETRIC COUPLING

So far, we have assumed that all coupling strengths are equal, $t_{\alpha,\beta} = t$. In practice, matching all couplings exactly might not be feasible; thus, it is important to investigate that our findings hold for systems with different couplings. We reproduced Fig. 3 with the couplings randomly varied in a window $\pm 20\%$ of the original $t = 0.2$ value shown in Fig. 5. The coupling terms $t_{\alpha,\beta}$ are numbered left to right, as shown by the double-sided gray arrows in Fig. 1(c). Here, t_1 (t_2) determines the coupling strength between the left QD and the left SC (middle SC), while t_3 (t_4) represents the

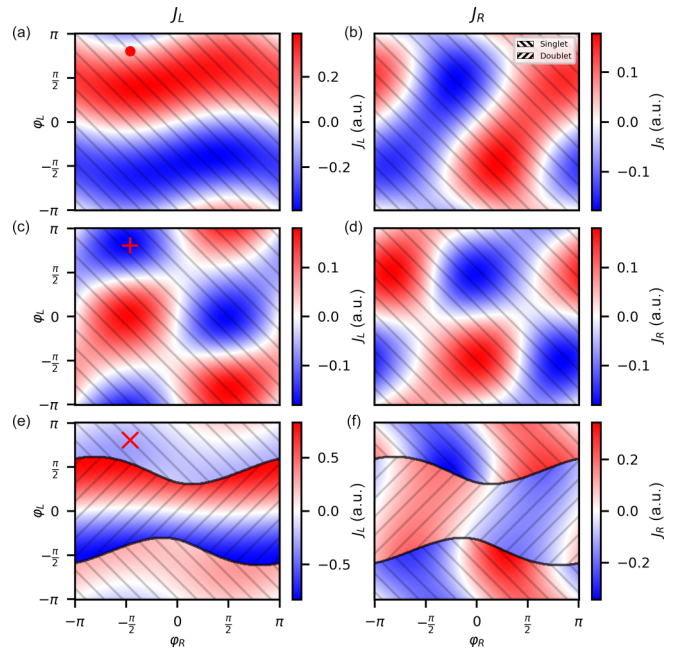


FIG. 7. The current of the nonlocal junction J_L and the local junction J_R , as a function of the local (φ_R) and nonlocal (φ_L) phase. For each row, the on-site energies are the same as for the same row of Fig. 4. The on-site energies where the current-phase relations (CPRs) are taken are marked with corresponding red marks in Fig. 2.

coupling between the right QD and the middle SC (right SC). Each row of Fig. 5 corresponds to a row of Fig. 3, with the same on-site energy and phase settings, but each panel of the row is generated with randomized values for $t_{\alpha,\beta}$; the exact values are shown above the panels. The color scale of each panel is normalized to that single panel to make all features visible. This makes the colors of different panels incomparable.

The first row shows the SC-QD-SC-like behavior, with two π phase shifts when the GS changes parity. We expect that the role of the SC phase between the two SC sites (φ_R between the middle and right SC site) will have a stronger effect when the coupling between the SC sites and the QD is stronger. Since the left QD is not on resonance, we only have to consider t_3 and t_4 , the coupling of the right QD to the two neighboring SC sites. When the couplings are strong, i.e., Fig. 5(b), we see that the local phase has a strong effect on the width of the doublet region; it is much narrower at $\varphi_R = 0$ than at $\varphi_R = \pi$. When the couplings are weak, i.e., Fig. 5(d), the width of the doublet region is much less affected by the phase, but the two cases are qualitatively the same.

The second row shows the case where the left dot is on resonance, with no phase applied to the nonlocal QD $\varphi_L = 0$. Here, we see the π phase shift in the doublet region around $\varepsilon_R = -0.8U$, discussed earlier, appear for all couplings.

The third and fourth rows show the cases where a finite phase is applied to the nonlocal QD, $\varphi_L \neq 0$. Here, again, we see the same features of Fig. 3, with the exact positions of the features shifting but still showing good qualitative agreement.

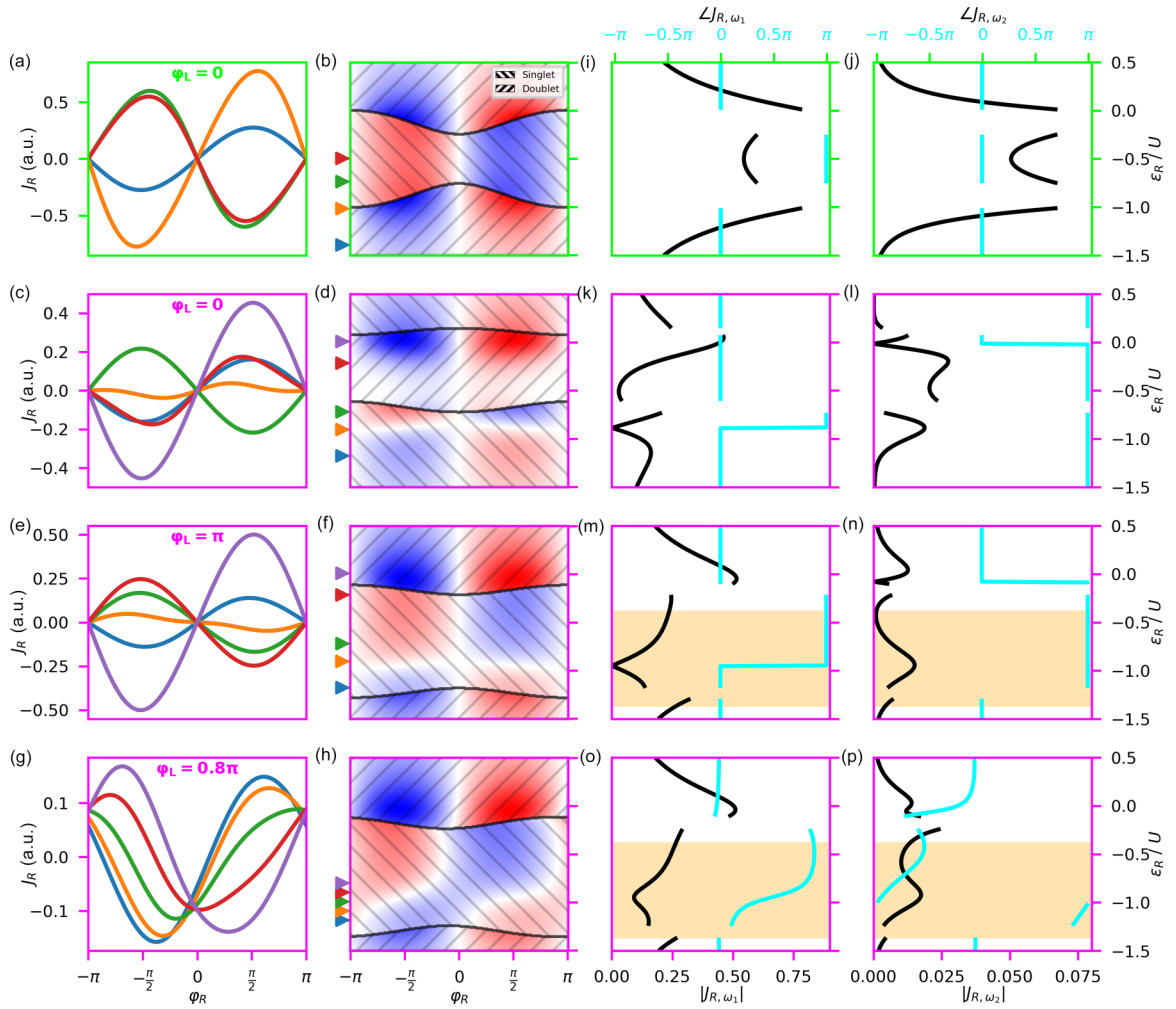


FIG. 8. Reproduction of Fig. 3, with the first and second harmonic parts of the current-phase relation (CPR) highlighted. The third column shows the first, the fourth column the second harmonic signal, with the black solid lines denoting the amplitude (bottom scale), the cyan lines the phase (top scale) of the signal. The lines are not continuous, where changing φ_R induces a ground state (GS) change, such as around $\varepsilon_R = 0$ and -1 in the first row.

APPENDIX B: SUPERCURRENT OF THE NONLOCAL QD

So far, we only concerned ourselves with the supercurrent flowing through the local QD J_R ; however, the roles of local and nonlocal QDs were arbitrarily set, and the roles could be easily reversed. In this section, we reproduce Figs. 3 and 4 with both J_R and J_L shown.

Figure 6(a) shows J_L when the left QD is not on resonance. Comparing the color bars of Figs. 6(a) and 6(b), we see that J_L is much smaller than J_R , as expected. The supercurrent in the left QD is also suppressed when the SC phase is set to $k\pi$, as shown in Figs. 6(c) and 6(e). If the left QD were not part of a larger system but the single QD of a SC-QD-SC system, we would expect the SC current to be zero. The fact that there is a finite current and its amplitude is tuned by the parameters of the other QD (φ_R, ε_R) is further evidence of the Andreev molecular states.

Figures 7(a) and 7(b) show that, when the on-site energies are tuned to the values shown by the red dot of Fig. 2, both QDs show the φ_0 phase shift discussed in the main text. When comparing Figs. 7(a) and 7(b), we must remember that,

if we wanted to reverse the roles of the local and nonlocal QDs of Fig. 7(a), in essence, we must exchange the φ_L and φ_R axes, which would mean mirroring the image along the $\varphi_L = \varphi_R$ diagonal. This is even more obvious for Figs. 7(c) and 7(d), where $\varepsilon_L = \varepsilon_R$, as shown by the red + of Fig. 2, and correspondingly, there is no distinction between the dots; mirroring one panel yields the other.

APPENDIX C: HIGHER HARMONICS OF THE SUPERCURRENT

In this section, we show how the first and second harmonic components of J_R are tuned separately. This helps us gain a deeper insight into the π -periodic CPRs as well as the φ_0 phase shifts shown in the main text. We are only concerned with the first two Fourier components, as the amplitude of higher harmonics is negligible. This means that we can write the supercurrent as $J_R \simeq J_{R,\omega_1} + J_{R,\omega_2} = |J_{R,\omega_1}| \sin(\varphi_R + \angle J_{R,\omega_1}) + |J_{R,\omega_2}| \sin(2\varphi_R + \angle J_{R,\omega_2})$.

As mentioned earlier, protected qubits based on systems with $\cos 2\varphi$ CPRs have been proposed [64]. This protection

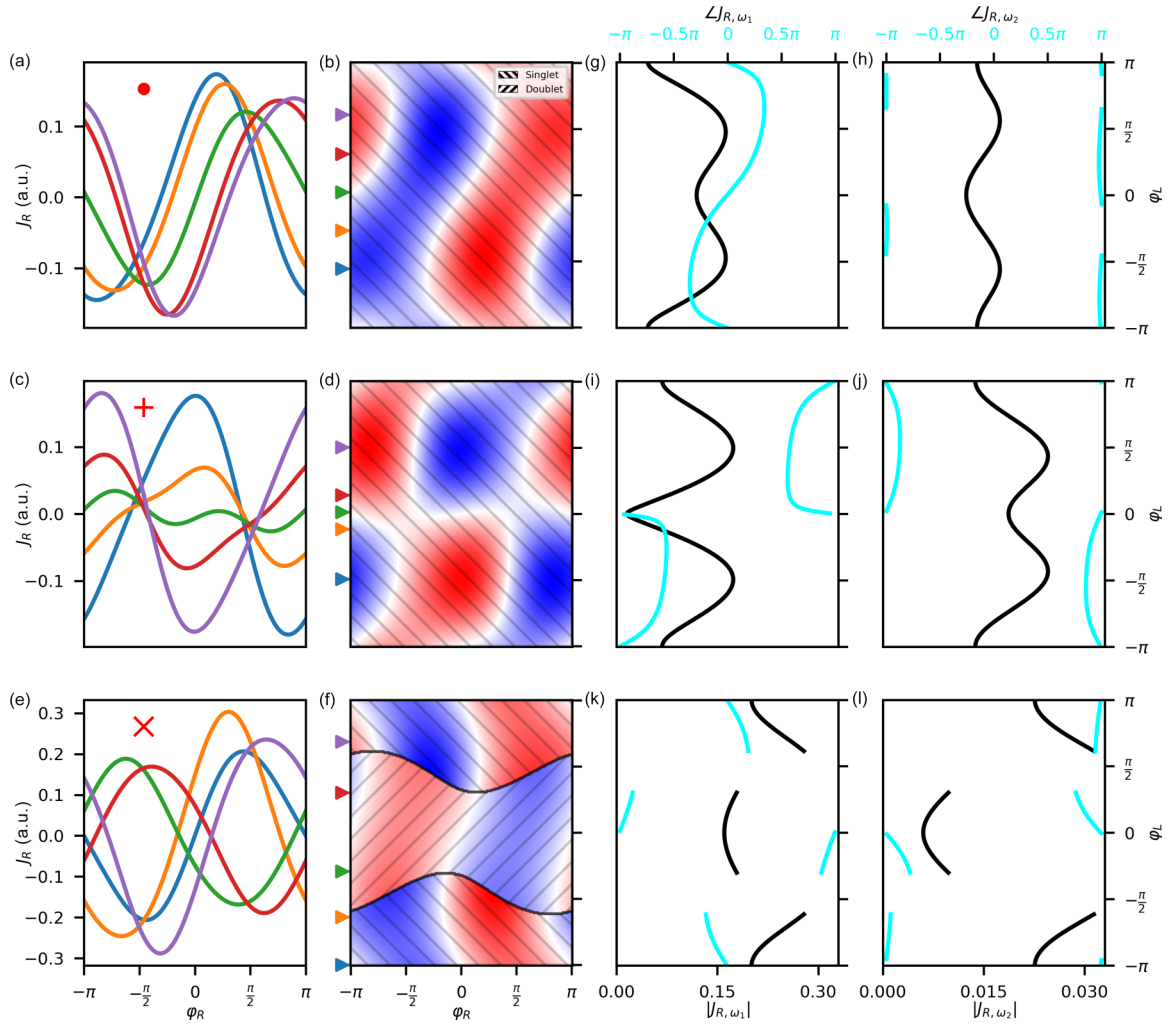


FIG. 9. Reproduction of Fig. 4, with the first and second harmonic parts of the current-phase relation (CPR) highlighted. The third column shows the first, the fourth column the second harmonic signal, with the black solid lines denoting the amplitude (bottom scale), the cyan lines the phase (top scale) of the signal. The lines are not continuous, where changing φ_R induces a ground state (GS) change, such as around $\varepsilon_R = 0$ and -1 in the first row.

requires that $J_{\omega_1} = 0$ and $J_{\omega_2} \neq 0$. However, if the suppression of the first harmonic signal is linear in a given parameter, $J_{\omega_1}(\alpha) \simeq \alpha$, it will be sensitive to the noise of that parameter, and the protection is lost. Ideally, in a protected state, the first harmonic component is suppressed at least quadratically in all parameters, $J_{\omega_1}(\alpha) \simeq \alpha^2$. Thus, we will look for such points in the parameter space.

Figure 8 is a reproduction of Fig. 3, with the addition of panels (i)–(p). The colors of the axes correspond to the value of ε_L shown in Fig. 2; the labels in the first column show the value of ε_L . The first column shows selected CPR curves and the supercurrent J_R (left scale) as a function of the local phase φ_R (bottom scale). The second column shows the supercurrent J_R as the function of the local phase φ_R (bottom scale) and local on-site energy ε_R (right scale). The third column corresponds to the first harmonic part of the CPR; the solid black line shows the amplitude (bottom scale), the cyan line the phase (top scale). The fourth column is like the third but shows the amplitude (black, bottom scale) and phase (cyan, top scale) of the second harmonic component of the signal.

1. Off-resonance case

The simplest case is that of the $0-\pi$ phase transition, when the nonlocal dot is off-resonance, as shown in the first row. Starting at the bottom of Fig. 8(b) [$\varepsilon_R < -1U$, blue and orange curves of Fig. 8(a)], we see that the phase of the first harmonic signal is 0. Above $\varepsilon_R \simeq -1U$ the CPR, $J_R(\varphi_R)$, curve shows jumps as singlet-doublet phase transitions are triggered when sweeping φ_R , so the Fourier decomposition of the CPR is not directly usable. This is why the curves of Figs. 8(i) and 8(j) are not continuous for values of ε_R , where changes in φ_R can trigger singlet-doublet transitions. Above $\varepsilon_R \simeq -0.75U$ [green curve and arrow in Figs. 8(a) and 8(b)], we see no jumps, but the CPRs are shifted by π , as shown by the jump in the red curve of Fig. 8(i). Around $\varphi_R \simeq 0$, we see a similar $0-\pi$ phase transition. The Fourier analysis of the first harmonic signal shows that the phase shift is indeed π , as described in the main text. This shows that decomposing the CPR signal is a good tool to determine the exact phase shift.

We also note that, while there is a nonnegligible second harmonic signal even in the off-resonant case, its amplitude

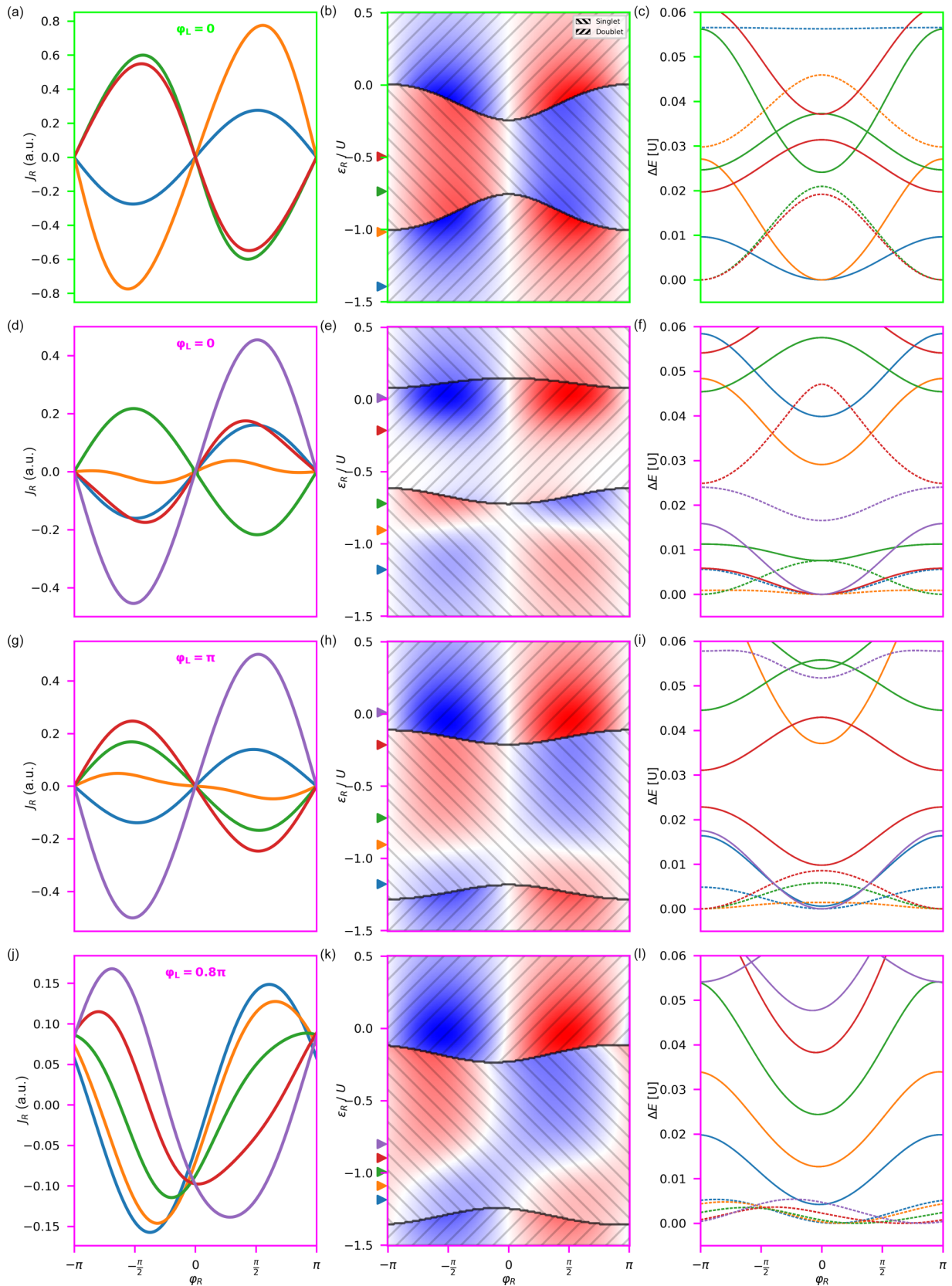


FIG. 10. Reproduction of Fig. 3, extended with the phase dependence of the energy of the lowest few levels (right column). For each spectra (each color), the minimum of the ground state energy was set to zero; ΔE is measured from this energy. Different colors denote spectra taken at different values of ϵ_R , as shown by the arrows of the same color on the middle column. Singlet states are shown with dashed lines, while degenerate (doublet or triplet) states are shown with a solid line.

is always smaller than that of the first harmonic part; thus, it only leads to the skewing of the signal.

2. Hybridization

The second and third rows of Fig. 8 show the nonlocal QD on resonance, and the nonlocal phase is 0 or π . In Secs. III B 2 and III B 3, we describe how a $0-\pi$ phase shift occurs without a singlet-doublet transition. Figures 8(k) and 8(m) show that the first harmonic singlet indeed has a π phase jump, when the amplitude goes to 0. Examining the same locations in Figs. 8(l) and 8(n), we see that the second harmonic signal has local maxima close to where the first harmonic goes to zero. This explains why the orange curves of Figs. 8(c) and 8(e) seem to be π periodic. The amplitude of the second harmonic signal is higher in the case of the red curve of Fig. 8(d), but since the first harmonic signal is not zero, it only manifests as the skewness of the CPR. The purple curve of the same panel has an even higher first harmonic component, while the second harmonic is zero, leading to a pure sinusoidal signal.

Here, we see that $J_{R,\omega_1} = 0$ and $J_{R,\omega_2} \neq 0$ [e.g., close to $\varepsilon_R = -1U$ in Figs. 8(m) and 8(n)]; however, the first harmonic signal depends linearly on ε_R close to its minimum, thus making the system susceptible to gate noise, in contrast with the protection requirement of the $\cos 2\varphi$ qubit.

3. φ_0 phase shift

The fourth row of Fig. 8 details the case of the φ_0 phase shift tuned by ε_R , when $\varphi_L = 0.8\pi$. Figure 8(o) shows how the exact value of the φ_0 phase shift of the CPR depends upon ε_R . It is also noteworthy that, unlike in the case of $\varphi_L = 0, \pi$, the amplitude of the first harmonic component of the CPR never goes to 0. Even though the amplitude of the second harmonic signal still has a local maximum at the minimum of the first harmonic signal since the latter does not go to 0, it only manifests as the skewness for the CPR curves.

4. Nonlocal phase tuning

For completeness, we also reproduce Fig. 4, extended with the amplitude and phase of the first and second harmonic signals, in Fig. 9 to help us further explore the effects of phase tuning. Here, we also see that, when the first harmonic signal disappears [see Fig. 9(i)], it does so linearly in φ_L , thus making the system susceptible to phase noise also.

APPENDIX D: ENERGY SPECTRA

While the main text of this paper focuses on the GS properties, the methods outlined can be used to calculate the excitation spectrum as well. The right column of Fig. 10 shows the energy spectra for the cases of Fig. 3. The spectra for different ε_R values are plotted as a function of φ_R with different colors, as indicated in the middle column by the arrows of the same color. For each spectrum (each color), the minimum of the GS energy was set to zero; ΔE is measured from this energy. We choose to show the same region of ΔE so that the details of the lower-energy states are still visible as well as some of the higher-energy states.

In Fig. 10(c), the GS of the blue and orange spectra are doublets (indicated by solid lines), while the red and green GSs are singlets (indicated by dashed lines), in accordance with the hatching of Fig. 10(b). One can also observe that, close to the $0-\pi$ flip, the singlet and doublet states are close to crossing, at $\varphi_R = 0$ for the green spectra and $\varphi_R = \pi$ for the orange. For the red and green cases, a third triplet state is also visible at higher energies.

In Fig. 10(f), we can see that the lowest blue (dashed) and red (solid) lines are close to overlapping, as are the CPRs of the two states shown in Fig. 10(d). It is also interesting to contrast the green and blue dotted lines of Fig. 10(f), where the phase dependence of the energy levels shifts by π while still being a singlet state. This is a consequence of the molecular state forming in the system, as we have discussed when we observed π transition of the current without parity change in the main text. The green cut was taken just below the value of ε_R , where the doublet state becomes the GS around $\varphi_R = 0$, which can also be seen by the dotted and solid green lines almost touching at $\varphi_R = 0$ in Fig. 10(f).

Comparing Figs. 10(f) and 10(i), one can see that there is a significant dependence on φ_L . The two panels show the spectra taken at the same values of ε_R , yet they are drastically different. This strong dependence on the nonlocal phase is also an indication of the molecular state encompassing both QDs.

Introducing an arbitrary phase difference in the left loop, e.g., $\varphi_L = 0.8\pi$ as shown in Fig. 10(l), introduces a φ_0 phase shift in the spectra, like the one observed in $J_R(\varphi_R)$ in Fig. 10(j).

-
- [1] J. D. Sau, R. M. Lutchyn, S. Tewari, and S. Das Sarma, Generic new platform for topological quantum computation using semiconductor heterostructures, *Phys. Rev. Lett.* **104**, 040502 (2010).
 - [2] R. M. Lutchyn, J. D. Sau, and S. Das Sarma, Majorana fermions and a topological phase transition in semiconductor-superconductor heterostructures, *Phys. Rev. Lett.* **105**, 077001 (2010).
 - [3] R. M. Lutchyn, E. P. A. M. Bakkers, L. P. Kouwenhoven, P. Krogstrup, C. M. Marcus, and Y. Oreg, Majorana zero modes in superconductor-semiconductor heterostructures, *Nat. Rev. Mater.* **3**, 52 (2018).
 - [4] C. Beenakker, Search for non-Abelian Majorana braiding statistics in superconductors, *SciPost Physics Lecture Notes* **15**, (2020).
 - [5] E. Prada, P. San-Jose, M. W. A. de Moor, A. Geresdi, E. J. H. Lee, J. Klinovaja, D. Loss, J. Nygård, R. Aguado, and L. P. Kouwenhoven, From Andreev to Majorana bound states in hybrid superconductor-semiconductor nanowires, *Nat. Rev. Phys.* **2**, 575 (2020).
 - [6] C. Nayak, S. H. Simon, A. Stern, M. Freedman, and S. Das Sarma, Non-Abelian anyons and topological quantum computation, *Rev. Mod. Phys.* **80**, 1083 (2008).

- [7] K. Flensberg, F. von Oppen, and A. Stern, Engineered platforms for topological superconductivity and Majorana zero modes, *Nat. Rev. Mater.* **6**, 944 (2021).
- [8] J. D. Sau and S. D. Sarma, Realizing a robust practical Majorana chain in a quantum-dot-superconductor linear array, *Nat. Commun.* **3**, 964 (2012).
- [9] M. Leijnse and K. Flensberg, Parity qubits and poor man's Majorana bound states in double quantum dots, *Phys. Rev. B* **86**, 134528 (2012).
- [10] A. Tsintzis, R. S. Souto, and M. Leijnse, Creating and detecting poor man's Majorana bound states in interacting quantum dots, *Phys. Rev. B* **106**, L201404 (2022).
- [11] T. Dvir, G. Wang, N. van Loo, C.-X. Liu, G. P. Mazur, A. Bordin, S. L. D. ten Haaf, J.-Y. Wang, D. van Driel, F. Zatelli *et al.*, Realization of a minimal Kitaev chain in coupled quantum dots, *Nature* **614**, 445 (2023).
- [12] L. Hofstetter, S. Csonka, J. Nygård, and C. Schönenberger, Cooper pair splitter realized in a two-quantum-dot Y-junction, *Nature (London)* **461**, 960 (2009).
- [13] L. G. Herrmann, F. Portier, P. Roche, A. L. Yeyati, T. Kontos, and C. Strunk, Carbon nanotubes as Cooper-pair beam splitters, *Phys. Rev. Lett.* **104**, 026801 (2010).
- [14] L. Hofstetter, S. Csonka, A. Baumgartner, G. Fülöp, S. d'Hollosy, J. Nygård, and C. Schönenberger, Finite-bias Cooper pair splitting, *Phys. Rev. Lett.* **107**, 136801 (2011).
- [15] A. Das, Y. Ronen, M. Heiblum, D. Mahalu, A. V. Kretinin, and H. Shtrikman, High-efficiency Cooper pair splitting demonstrated by two-particle conductance resonance and positive noise cross-correlation, *Nat. Commun.* **3**, 1165 (2012).
- [16] J. Schindele, A. Baumgartner, and C. Schönenberger, Near-unity Cooper pair splitting efficiency, *Phys. Rev. Lett.* **109**, 157002 (2012).
- [17] N. J. Lambert, M. Edwards, A. A. Esmail, F. A. Pollock, S. D. Barrett, B. W. Lovett, and A. J. Ferguson, Experimental observation of the breaking and recombination of single Cooper pairs, *Phys. Rev. B* **90**, 140503(R) (2014).
- [18] Z. B. Tan, D. Cox, T. Nieminen, P. Lähteenmäki, D. Golubev, G. B. Lesovik, and P. J. Hakonen, Cooper pair splitting by means of graphene quantum dots, *Phys. Rev. Lett.* **114**, 096602 (2015).
- [19] M. R. Buitelaar, T. Nussbaumer, and C. Schönenberger, Quantum dot in the Kondo regime coupled to superconductors, *Phys. Rev. Lett.* **89**, 256801 (2002).
- [20] A. Eichler, M. Weiss, S. Oberholzer, C. Schönenberger, A. Levy Yeyati, J. C. Cuevas, and A. Martín-Rodero, Even-odd effect in Andreev transport through a carbon nanotube quantum dot, *Phys. Rev. Lett.* **99**, 126602 (2007).
- [21] T. Sand-Jespersen, J. Paaske, B. M. Andersen, K. Grove-Rasmussen, H. I. Jørgensen, M. Aagesen, C. B. Sørensen, P. E. Lindelof, K. Flensberg, and J. Nygård, Kondo-enhanced Andreev tunneling in InAs nanowire quantum dots, *Phys. Rev. Lett.* **99**, 126603 (2007).
- [22] R. S. Deacon, Y. Tanaka, A. Oiwa, R. Sakano, K. Yoshida, K. Shibata, K. Hirakawa, and S. Tarucha, Tunneling spectroscopy of Andreev energy levels in a quantum dot coupled to a superconductor, *Phys. Rev. Lett.* **104**, 076805 (2010).
- [23] J.-D. Pillet, C. H. L. Quay, P. Morfin, C. Bena, A. L. Yeyati, and P. Joyez, Andreev bound states in supercurrent-carrying carbon nanotubes revealed, *Nat. Phys.* **6**, 965 (2010).
- [24] R. Maurand, T. Meng, E. Bonet, S. Florens, L. Marty, and W. Wernsdorfer, First-order $0-\pi$ quantum phase transition in the Kondo regime of a superconducting carbon-nanotube quantum dot, *Phys. Rev. X* **2**, 011009 (2012).
- [25] E. J. H. Lee, X. Jiang, R. Aguado, G. Katsaros, C. M. Lieber, and S. De Franceschi, Zero-bias anomaly in a nanowire quantum dot coupled to superconductors, *Phys. Rev. Lett.* **109**, 186802 (2012).
- [26] A. Kumar, M. Gaim, D. Steininger, A. Levy Yeyati, A. Martín-Rodero, A. K. Hüttel, and C. Strunk, Temperature dependence of Andreev spectra in a superconducting carbon nanotube quantum dot, *Phys. Rev. B* **89**, 075428 (2014).
- [27] E. J. H. Lee, X. Jiang, M. Houzet, R. Aguado, C. M. Lieber, and S. De Franceschi, Spin-resolved Andreev levels and parity crossings in hybrid superconductor-semiconductor nanostructures, *Nat. Nanotechnol.* **9**, 79 (2014).
- [28] J. Schindele, A. Baumgartner, R. Maurand, M. Weiss, and C. Schönenberger, Non-local spectroscopy of Andreev bound states, *Phys. Rev. B* **89**, 045422 (2014).
- [29] A. Jellinggaard, K. Grove-Rasmussen, M. H. Madsen, and J. Nygård, Tuning Yu-Shiba-Rusinov states in a quantum dot, *Phys. Rev. B* **94**, 064520 (2016).
- [30] J. Gramich, A. Baumgartner, and C. Schönenberger, Andreev bound states probed in three-terminal quantum dots, *Phys. Rev. B* **96**, 195418 (2017).
- [31] L. Bretheau, J. I.-J. Wang, R. Pisoni, K. Watanabe, T. Taniguchi, and P. Jarillo-Herrero, Tunnelling spectroscopy of Andreev states in graphene, *Nat. Phys.* **13**, 756 (2017).
- [32] D. J. van Woerkom, A. Proutski, B. van Heck, D. Bouman, J. I. Väyrynen, L. I. Glazman, P. Krogstrup, J. Nygård, L. P. Kouwenhoven, and A. Geresdi, Microwave spectroscopy of spinful Andreev bound states in ballistic semiconductor Josephson junctions, *Nat. Phys.* **13**, 876 (2017).
- [33] M. Hays, G. de Lange, K. Serniak, D. J. van Woerkom, D. Bouman, P. Krogstrup, J. Nygård, A. Geresdi, and M. H. Devoret, Direct microwave measurement of Andreev-bound-state dynamics in a semiconductor-nanowire Josephson junction, *Phys. Rev. Lett.* **121**, 047001 (2018).
- [34] D. Laroche, D. Bouman, D. J. van Woerkom, A. Proutski, C. Murthy, D. I. Pikulin, C. Nayak, R. J. J. van Gulik, J. Nygård, P. Krogstrup *et al.*, Observation of the 4π -periodic Josephson effect in indium arsenide nanowires, *Nat. Commun.* **10**, 245 (2019).
- [35] J. C. Estrada Saldaña, A. Vekris, V. Sosnovtseva, T. Kanne, P. Krogstrup, K. Grove-Rasmussen, and J. Nygård, Temperature induced shifts of Yu-Shiba-Rusinov resonances in nanowire-based hybrid quantum dots, *Commun. Phys.* **3**, 1 (2020).
- [36] J.-D. Pillet, V. Benzoni, J. Griesmar, J.-L. Smirr, and C. O. Girit, Nonlocal Josephson effect in Andreev molecules, *Nano Lett.* **19**, 7138 (2019).
- [37] J.-D. Pillet, V. Benzoni, J. Griesmar, J.-L. Smirr, and C. O. Girit, Scattering description of Andreev molecules, *SciPost Physics Core* **2**, 009 (2020).
- [38] Z. Scherübl, A. Pályi, and S. Csonka, Transport signatures of an Andreev molecule in a quantum dot-superconductor-quantum dot setup, *Beilstein J. Nanotechnol.* **10**, 363 (2019).
- [39] V. Kornich, H. S. Barakov, and Y. V. Nazarov, Fine energy splitting of overlapping Andreev bound states in multiterminal superconducting nanostructures, *Phys. Rev. Res.* **1**, 033004 (2019).

- [40] V. Kornich, H. S. Barakov, and Y. V. Nazarov, Overlapping Andreev states in semiconducting nanowires: Competition of 1D and 3D propagation, *Phys. Rev. B* **101**, 195430 (2020).
- [41] M. Coraiola, D. Z. Haxell, D. Sabonis, H. Weisbrich, A. E. Svetogorov, M. Hinderling, S. C. ten Kate, E. Cheah, F. Krizek, R. Schott *et al.*, Phase-engineering of the Andreev band structure of a three-terminal Josephson junction, *Nat. Commun.* **14**, 6784 (2023).
- [42] O. Kürtössy, Z. Scherübl, G. Fülöp, I. E. Lukács, T. Kanne, J. Nygård, P. Makk, and S. Csonka, Andreev molecule in parallel InAs nanowires, *Nano Lett.* **21**, 7929 (2021).
- [43] S. Matsuo, T. Imoto, T. Yokoyama, Y. Sato, T. Lindemann, S. Gronin, G. C. Gardner, S. Nakosai, Y. Tanaka, M. J. Manfra *et al.*, Phase-dependent Andreev molecules and superconducting gap closing in coherently-coupled Josephson junctions, *Nat. Commun.* **14**, 8271 (2023).
- [44] A. A. Reynoso, G. Usaj, C. A. Balseiro, D. Feinberg, and M. Avignon, Anomalous Josephson current in junctions with spin-polarizing quantum point contacts, *Phys. Rev. Lett.* **101**, 107001 (2008).
- [45] A. Buzdin, Direct coupling between magnetism and superconducting current in Josephson φ_0 junction, *Phys. Rev. Lett.* **101**, 107005 (2008).
- [46] A. Zazunov, R. Egger, T. Jonckheere, and T. Martin, Anomalous Josephson current through a spin-orbit coupled quantum dot, *Phys. Rev. Lett.* **103**, 147004 (2009).
- [47] E. Goldobin, D. Koelle, R. Kleiner, and R. G. Mints, Josephson junction with magnetic-field tunable ground state, *Phys. Rev. Lett.* **107**, 227001 (2011).
- [48] H. Sickinger, A. Lipman, M. Weides, R. G. Mints, H. Kohlstedt, D. Koelle, R. Kleiner, and E. Goldobin, Experimental evidence of a φ Josephson junction, *Phys. Rev. Lett.* **109**, 107002 (2012).
- [49] T. Yokoyama, M. Eto, and Y. V. Nazarov, Anomalous Josephson effect induced by spin-orbit interaction and Zeeman effect in semiconductor nanowires, *Phys. Rev. B* **89**, 195407 (2014).
- [50] A. A. Golubov, M. Y. Kupriyanov, and E. Il'ichev, The current-phase relation in Josephson junctions, *Rev. Mod. Phys.* **76**, 411 (2004).
- [51] Y. M. Shukrinov, Anomalous Josephson effect, *Phys. Usp.* **65**, 317 (2022).
- [52] D. B. Szombati, S. Nadj-Perge, D. Car, S. R. Plissard, E. P. A. M. Bakkers, and L. P. Kouwenhoven, Josephson φ_0 -junction in nanowire quantum dots, *Nat. Phys.* **12**, 568 (2016).
- [53] W. Mayer, M. C. Dartiaillh, J. Yuan, K. S. Wickramasinghe, E. Rossi, and J. Shabani, Gate controlled anomalous phase shift in Al/InAs Josephson junctions, *Nat. Commun.* **11**, 212 (2020).
- [54] S. Pal and C. Benjamin, Quantized Josephson phase battery, *Europhys. Lett.* **126**, 57002 (2019).
- [55] E. Strambini, A. Iorio, O. Durante, R. Citro, C. Sanz-Fernández, C. Guarcello, I. V. Tokatly, A. Braggio, M. Rocci, N. Ligato *et al.*, A Josephson phase battery, *Nat. Nanotechnol.* **15**, 656 (2020).
- [56] G. O. Steffensen, Yu-Shiba-Rushinov Bound States in Quantum Dots, Master's thesis, Københavns Universitet Niels Bohr Institute (2017).
- [57] G. Steffensen, YSR States in Double Quantum Dots, Ph.D. thesis, Københavns Universitet Niels Bohr Institute (2021).
- [58] C. Hermansen, A. L. Yeyati, and J. Paaske, Inductive microwave response of Yu-Shiba-Rusinov states, *Phys. Rev. B* **105**, 054503 (2022).
- [59] J. A. van Dam, Y. V. Nazarov, E. P. A. M. Bakkers, S. De Franceschi, and L. P. Kouwenhoven, Supercurrent reversal in quantum dots, *Nature (London)* **442**, 667 (2006).
- [60] A. Bargerbos, M. Pita-Vidal, R. Žitko, J. Ávila, L. J. Splitthoff, L. Grünhaupt, J. J. Wesdorp, C. K. Andersen, Y. Liu, L. P. Kouwenhoven *et al.*, Singlet-doublet transitions of a quantum dot Josephson junction detected in a transmon circuit, *PRX Quantum* **3**, 030311 (2022).
- [61] A. Leblanc, C. Tangchingchai, Z. S. Momtaz, E. Kiyooka, J.-M. Hartmann, G. T. Fernandez-Bada, B. Brun-Barriere, V. Schmitt, S. Zihlmann, R. Maurand *et al.*, From nonreciprocal to charge-4e supercurrents in Ge-based Josephson devices with tunable harmonic content, [arXiv:2311.15371](https://arxiv.org/abs/2311.15371).
- [62] C. Ciaccia, R. Haller, A. C. C. Drachmann, T. Lindemann, M. J. Manfra, C. Schrade, and C. Schönenberger, Charge-4e supercurrent in a two-dimensional InAs-Al superconductor-semiconductor heterostructure, *Commun. Phys.* **7**, 41 (2024).
- [63] M. Valentini, O. Sagi, L. Baghumyan, T. de Gijssel, J. Jung, S. Calcaterra, A. Ballabio, J. Aguilera Servin, K. Aggarwal, M. Janik *et al.*, Parity-conserving Cooper-pair transport and ideal superconducting diode in planar germanium, *Nat. Commun.* **15**, 169 (2024).
- [64] C. Schrade, C. M. Marcus, and A. Gyenis, Protected hybrid superconducting qubit in an array of gate-tunable Josephson interferometers, *PRX Quantum* **3**, 030303 (2022).
- [65] A. A. Reynoso, G. Usaj, C. A. Balseiro, D. Feinberg, and M. Avignon, Spin-orbit induced chirality of Andreev states in Josephson junctions, *Phys. Rev. B* **86**, 214519 (2012).
- [66] R. Wakatsuki, Y. Saito, S. Hoshino, Y. M. Itahashi, T. Ideue, M. Ezawa, Y. Iwasa, and N. Nagaosa, Nonreciprocal charge transport in noncentrosymmetric superconductors, *Sci. Adv.* **3**, e1602390 (2017).
- [67] G. P. Mazur, N. van Loo, D. van Driel, J.-Y. Wang, G. Badawy, S. Gazibegovic, E. P. A. M. Bakkers, and L. P. Kouwenhoven, The gate-tunable Josephson diode, [arXiv:2211.14283](https://arxiv.org/abs/2211.14283).
- [68] C. Baumgartner, L. Fuchs, A. Costa, S. Reinhardt, S. Gronin, G. C. Gardner, T. Lindemann, M. J. Manfra, P. E. Faria Junior, D. Kochan *et al.*, Supercurrent rectification and magnetochiral effects in symmetric Josephson junctions, *Nat. Nanotechnol.* **17**, 39 (2022).
- [69] H. Wu, Y. Wang, Y. Xu, P. K. Sivakumar, C. Pasco, U. Filippozzi, S. S. P. Parkin, Y.-J. Zeng, T. McQueen, and M. N. Ali, The field-free Josephson diode in a van der Waals heterostructure, *Nature (London)* **604**, 653 (2022).
- [70] M. Gupta, G. V. Graziano, M. Pendharkar, J. T. Dong, C. P. Dempsey, C. Palmstrøm, and V. S. Pribiag, Gate-tunable superconducting diode effect in a three-terminal Josephson device, *Nat. Commun.* **14**, 3078 (2023).
- [71] C. Ciaccia, R. Haller, A. C. C. Drachmann, T. Lindemann, M. J. Manfra, C. Schrade, and C. Schönenberger, Gate-tunable Josephson diode in proximitized InAs supercurrent interferometers, *Phys. Rev. Res.* **5**, 033131 (2023).
- [72] J.-D. Pillet, S. Annabi, A. Peugeot, H. Riechert, E. Arrighi, J. Griesmar, and L. Bretheau, Josephson diode effect in Andreev molecules, *Phys. Rev. Res.* **5**, 033199 (2023).
- [73] M. Nadeem, M. S. Fuhrer, and X. Wang, The superconducting diode effect, *Nat. Rev. Phys.* **5**, 558 (2023).
- [74] M. Pita-Vidal, A. Bargerbos, R. Žitko, L. J. Splitthoff, L. Grünhaupt, J. J. Wesdorp, Y. Liu, L. P. Kouwenhoven, R. Aguado, B. van Heck *et al.*, Direct manipulation of a

- superconducting spin qubit strongly coupled to a transmon qubit, *Nat. Phys.* **19**, 1110 (2023).
- [75] S. Matsuo, J. S. Lee, C.-Y. Chang, Y. Sato, K. Ueda, C. J. Palmstrøm, and S. Tarucha, Observation of nonlocal Josephson effect on double InAs nanowires, *Commun. Phys.* **5**, 221 (2022).
- [76] J. J. Wesdorp, F. J. Matute-Cañadas, A. Vaartjes, L. Grünhaupt, T. Laeven, S. Roelofs, L. J. Splitthoff, M. Pita-Vidal, A. Bargerbos, D. J. van Woerkom *et al.*, Microwave spectroscopy of interacting Andreev spins, *Phys. Rev. B* **109**, 045302 (2024).
- [77] J. S. Lee, B. Shojaei, M. Pendharkar, A. P. McFadden, Y. Kim, H. J. Suominen, M. Kjaergaard, F. Nichele, H. Zhang, C. M. Marcus *et al.*, Transport studies of Epi-Al/InAs two-dimensional electron gas systems for required building-blocks in topological superconductor networks, *Nano Lett.* **19**, 3083 (2019).
- [78] A. Bargerbos, M. Pita-Vidal, R. Žitko, L. J. Splitthoff, L. Grünhaupt, J. J. Wesdorp, Y. Liu, L. P. Kouwenhoven, R. Aguado, C. K. Andersen *et al.*, Spectroscopy of spin-split Andreev levels in a quantum dot with superconducting leads, *Phys. Rev. Lett.* **131**, 097001 (2023).
- [79] D. Z. Haxell, M. Coraiola, M. Hinderling, S. C. ten Kate, D. Sabonis, A. E. Svetogorov, W. Belzig, E. Cheah, F. Krizek, R. Schott *et al.*, Demonstration of nonlocal Josephson effect in Andreev molecules, *Nano Lett.* **23**, 7532 (2023).
- [80] S. Matsuo, T. Imoto, T. Yokoyama, Y. Sato, T. Lindemann, S. Gronin, G. C. Gardner, M. J. Manfra, and S. Tarucha, Phase engineering of anomalous Josephson effect derived from Andreev molecules, *Sci. Adv.* **9**, eadj3698 (2023).
- [81] S. Matsuo, T. Imoto, T. Yokoyama, Y. Sato, T. Lindemann, S. Gronin, G. C. Gardner, M. J. Manfra, and S. Tarucha, Josephson diode effect derived from short-range coherent coupling, *Nat. Phys.* **19**, 1636 (2023).
- [82] E. W. Hodt and J. Linder, On-off switch and sign change for non-local Josephson diode in spin-valve Andreev molecules, *Phys. Rev. B* **108**, 174502 (2023).